Journal of Structural Geology, Vol. 15, No. 2, pp. 129 to 144, 1993
Printed in Great Britain

0191-8141/93 $06.00+0.00

Microstructures, deformation mechanisms and strain patterns in a vertical profile, inner Appalachian fold–thrust belt, Alabama

SCHUMAN WU

CogniSeis Development, 1800 30th Street, Suite 304, Boulder, CO 80301, U.S.A.

(*Received* 28 *August* 1991; *accepted in revised form* 13 *July* 1992)

Abstract—A core from the American Anniston No. 1 well, drilled in the Pell City thrust sheet, Calhoun County, Alabama, provides an excellent scientific opportunity to study in a vertical profile the deformation mechanisms and strain patterns associated with large-scale structures. The core contains stratigraphic units from Cambrian to Mississippian in age and two major thrust faults. A detailed structural analysis revealed two deformation episodes, a pre-orogenic deformation and Alleghanian orogenic deformation. In the pre-orogenic deformation, synsedimentary folds and growth faults are the characteristic early structures, and normal faults formed in lithifield rocks later. During Alleghanian deformation, earlier fractures are overprinted by later S_1 penetrative structures. In limestone, shale and siltstone within thrust sheets, S_1 is solution cleavage. Dolomites in the thrust sheets were deformed by fracturing, and no penetrative cleavages formed. In major fault zones, S_1 mylonitic foliation formed in limestone, shale and siltstone. Fault-related dolomites were deformed cataclastically and no S surfaces formed. Strain magnitude increases towards major thrust faults in both the hanging walls and footwalls. For the typical fault configuration in the core with limestone–dolomite in the hanging wall and shale–siltstone in the footwall, strain is mainly caused by pressure solution and cataclasis in the hanging wall and by plastic deformation in the footwall.

INTRODUCTION

FROM foreland to hinterland across a fold–thrust belt, structural styles and strain patterns at a large scale and deformation mechanisms at a microscopic scale change significantly (Fellows 1943, Cloos 1947, Groshong *et al.* 1984, Mitra 1987, Evans & Dunne 1991, Wu & Groshong 1991). Across such a transect the deformation usually changes from brittle to semi-brittle or ductile with increasing intensity (Mitra 1987, Evans & Dunne 1991). Also, frontal parts of a fold–thrust belt may experience single episode of deformation (Wu & Groshong 1991), whereas in the internal portions of a belt, such as at front of the Blue Ridge province of the central Appalachians (Gibson & Gray 1985, Mitra 1987, Chester 1989, Evans & Dunne 1991) and the leading edge of Talladega slate belt in the southern Appalachians (Guthrie 1990), the deformation history usually involves multiple episodes.

These lateral changes have been established across fold–thrust belts, but what are the vertical changes from within a thrust sheet to a fault zone? Are they comparable? Answers to these questions have been difficult to obtain because of the lack of sufficient vertical exposure at single locations. This paper uses a 914-m (3000 ft) continuous core, drilled by Amoco near Anniston, Alabama, to attempt to address these questions. The well is at a critical position in the regional geology where the structural and stratigraphic transitions occur between the Valley and Ridge province and the Talladega slate belt (Fig. 1a). The core contains rocks of stratigraphic units of the Valley and Ridge province, two major thrusts faults of regional significance, and four or five small thrust faults (Fig. 2).

This study addresses: (1) the sequence of microstructures, to reveal multiple generations of microstructures or progressive deformation (Watts & Williams 1979, Powell & Richard 1985,Williams 1985, Wilson & de Hedouville 1985) that can be related to evolution of a thrust system (Marshak & Engelder 1985, Mitra & Yonkee 1985); (2) changes in deformation mechanisms

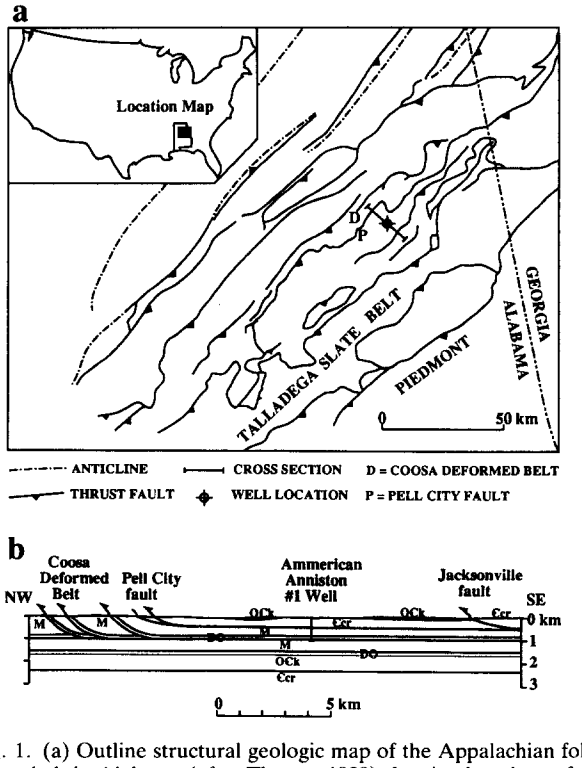

Fig. 1. (a) Outline structural geologic map of the Appalachian fold–thrust belt in Alabama (after Thomas 1989) showing locations of the American Anniston No. 1 well. (b) Cross-section through the American Anniston No. 1 well. Surface geology is based on the Geologic Map of Alabama (Szabo *et al.* 1988). Abbreviations: M, Mississippian; DO, Devonian and Ordovician; O-Ck, Cambrian–Ordovician Knox Formation; -Ccr, Cambrian Conasauga Formation and Rome Formation.

and strain pattern with depth, across thrust faults and among different rock types (Mitra 1984, Gibson & Gray 1985), different depths of burial (Miller *et al.* 1983, Harper 1985); and (3) strain partitioning among different deformation mechanisms (Ramsay & Huber 1983, Groshong *et al.* 1984, Evans & Dunne 1991) to reveal their contributions to the finite strain.

In this paper, the term microstructures will be used to include structures identified both on a microscopic scale (under a microscope) and mesoscopic scale (observable in a hand sample or thin section with or without a hand lens) as defined by Turner & Weiss (1963). Following the discussion of Rutter (1986), the terms cataclastic and plastic are used to describe deformation mechanisms; and the terms brittle and ductile are used to describe structural styles. Cataclastic fracturing includes fracturing, faulting, and vein formation (in which extensional or shear fractures are filled). Cataclasis is used to describe the process of formation of cataclasite, in which grain sizes are substantially reduced (Stearns 1969, Tullis & Yund 1987, Hanmer 1989).

The terminology of Sibson (1977) for subdivision of mylonite and cataclasite is followed with some modifications. For cohesive fault-zone rocks with significant amount of tectonic matrix, whether the term cataclasite or mylonite is applied depends on the dominant deformation mechanisms. If cataclastic mechanisms (frictional sliding, fracturing, etc.) dominated the deformation, the rock is classified as cataclasite regardless of whether it is foliated or not. If plastic mechanisms (such as translation gliding, grain boundary migration, diffusion, recrystallization, etc.) dominated the deformation and contribute to the primary rock fabric, the rock is classified as mylonite. Mylonites are mostly foliated (Wise *et al.* 1984, Groshong 1988).

GEOLOGIC SETTING, STRATIGRAPHY AND STRUCTURES

The American Anniston No. 1 well penetrates the Pell City thrust sheet (Fig. 1) near Anniston, Alabama,

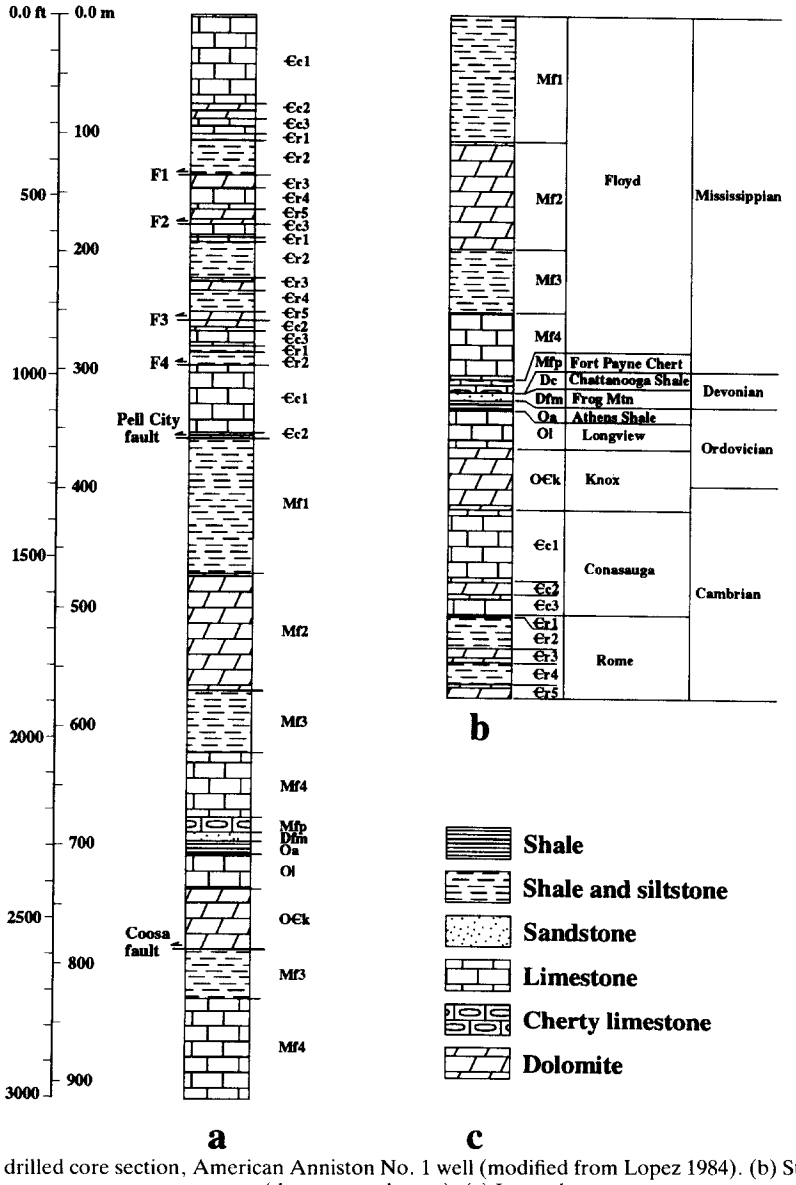

Fig. 2. (a) The drilled core section, American Anniston No. 1 well (modified from Lopez 1984). (b) Stratigraphic column (the same scale as a). (c) Legend.

which is in the internal part of the Valley and Ridge province of southern Appalachians in Alabama. The well was drilled at the hinge of a local anticline (Fig. 1) in poorly exposed Cambrian Conasauga limestone and shale. It crosses two major thrust faults that placed Cambrian carbonates on top of Mississippian clastics (Fig. 2a). One is at 350 m (1180 ft) below the surface and is correlated with the Pell City thrust fault. The other is at 790 m (2590 ft) and correlates with one of the thrust faults in the Coosa deformed belt (Fig. 1b). Also, four small thrust faults are encountered in the hanging wall of the Pell City fault. All structures belong to the Valley and Ridge province and formed in the Alleghanian orogeny (Mississippian to Permian).

The preliminary stratigraphic and structural analyses of the core are provided by Lopez (1984). The total stratigraphic thickness repeated in the 914-m (3000 ft) core (Fig. 2a) is about 365–475 m (1200–1560 ft) (Fig. 2b). Table 1 summarizes stratigraphy and lithology which are modified from Lopez (1984). Use of the Devonian Frog Mountain Formation (Dfm) is suggested by William A. Thomas (personal communication 1989). The dolomite of the Mississippian Floyd Formation is treated as a member instead of a facies change of the limestone member. According to Thomas (1972), interbedding of shale and carbonate rocks is characteristic in the Floyd Formation in this area, and so, evidence does not support facies change between dolomite and limestone.

The Pell City fault, with a strike length of at least 120 km, is a major structure in the internal Valley and Ridge province of Alabama (Fig. 1). Fault displacement is estimated to be 22–25 km at the well location from the balanced cross-sections (Thomas 1985). In the core, an irregular fault contact zone 0.45-m (1.5 ft) thick separates the Conasauga dolomite and the Floyd shale. A 0.2-m (8 in.) ultracataclasite zone, which is composed of very fine-grained granulated matrix, is found within the fault contact. The composition of the ultracataclasite determined by X-ray diffraction is estimated to be 86% ferrodolomite, 6% quartz, 6% calcite and 2% illite–mica (Lopez 1984). The Conasauga dolomite (Ꞓc2) above the fault is intensely fractured. In the footwall, Mississippian Floyd shale and siltstone (120 m or 400 ft) are mylonitic and strongly foliated by aligned platy clay minerals (chlorite and illite) and quartz–calcite augens and ribbons. The parting surfaces of the foliation are highly polished and striated. Quartz and calcite are completely recrystallized within the augens and ribbons. Original sedimentary structures were erased in the Floyd mylonite.

The Coosa-equivalent thrust, F_7, has a displacement of 5–6 km from the balanced cross-sections (Thomas 1985). Within the fault contact there is 0.6-m (2 ft) thick ultracataclasite similar to that of Pell City fault, F_5. The approximate composition of fault rocks at 789 m (or 2588 ft) from X-ray diffraction is 38% calcite, 32% dolomite, 27% ferrodolomite and 3% quartz (Lopez 1984). The dolomite (OꞒk) above the fault is intensely fractured and the shale and siltstone (Mf3, 39 m or 129 ft) in the footwall are strongly foliated similar to that in the footwall of Pell City fault.

Faults F_1–F_4 imbricate the Cambrian Rome and Conasauga section in the Pell City thrust sheet. F_1 is a minor fault with 0.25-m (10 in.) siliceous cataclasite. Bedding-parallel faults suggest that deformation above and below the fault zone is characterized by bedding slip within siltstone and shale. F_2 has a 0.9-m (3 ft) cataclastic fault zone between basal Rome dolomite and basal Conasauga limestone. Fractures extend throughout the dolomite (Ꞓr5, 10 m or 34 ft). The overlying sandstone is moderately fractured. Fracture intensity in the footwall

Table 1. Stratigraphy and lithology

Age	Formation		Lithology
Mississippian	Floyd	Mf1	Black shale with siltstone units
		Mf2	Fine to coarse crystalline dolomite
		Mf3	Black shale with siltstone units
		Mf4	Fossiliferous limestone
	Fort Payne Chert	Mfp	Light gray chert
Devonian	Chattanooga Shale	Dc	Brownish to black organic shale
	Frog Mtn	Dfm	Medium to fine quartz sandstone
Ordovican	Athens Shale	Oa	Black shale
	Longview	Ol	Marly limestone, chert, microcrystalline limestone interbedded with argillaceous limestone
	Knox	OꞒk	Fine to coarse crystalline dolomite
Cambrian	Conasauga	Ꞓc1	Interbedded pisolitic grainstone and calcareous mudstone
		Ꞓc2	Fine crystalline dolomitic mudstone
		Ꞓc3	Interbedded pisolitic grain stone and calcareous mudstone
	Rome	Ꞓr1	Green shale
		Ꞓr2	Shale and siltstone, finely interbedded
		Ꞓr3	Dolomite, poorly bedded
		Ꞓr4	Shale and siltstone, finely interbedded
		Ꞓr5	Dolomite, poorly bedded

limestone is low, and fault-related fractures extend no more than 1 m below the fault zone. F_3 placed basal Rome dolomite above middle Conasauga dolomite. The fault is a planar surface between the hanging wall and the footwall. Fractures extend 8.5 m (28 ft) into the hanging wall. The footwall contains a 0.08-m (3 in.) cataclasite, and no fractures extend beyond 0.9 m (3 ft) below the fault. F_4 has a 0.6-m (2 ft) fault zone, and placed upper Rome siltstone on upper Conasauga limestone. The fault zone contains cataclasite and protocataclasite. X-ray diffraction analysis of the fault zone material estimates 34% chlorite, 19% quartz, 17% illite, 13% feldspar, 10% ferrodolomite, 5% pyrite and 2% calcite (Lopez 1984). A 0.6-m thick dolomite above the fault is intensely fractured. Fracture intensity in the siltstone above the dolomite is small, but polishing and striation on bedding partings indicate bedding-slip. Fractures due to F_4 do not extend more than 0.6 m into the footwall limestone (Ꞓc1).

MICROSTRUCTURE SEQUENCE

In this section, microstructures in the core will be shown to have formed during two deformation episodes, a pre-orogenic extensional tectonism and the Alleghanian orogeny. In each deformation episode, the possible microstructure sequence is also discussed.

In the pre-orogenic deformation, bedding and bedding-parallel stylolites formed during sedimentation and burial diagenesis. Synsedimentary structures include soft-sediment folds and growth faults (Fig. 3a). Most synsedimentary structures are found in the weakly deformed Cambrian Rome Formation from the middle of the Pell City thrust sheet. Subsequently consolidated rocks of Rome Formation (Fig. 3b) as well as in Floyd siltstone, dolomite and Knox dolomite were offset by normal faults. The sharp fault surfaces, similar bed thickness in hanging walls and footwalls, and no drag along fault surfaces distinguish these normal faults. Also, the high-angle dips and occurrence only in weakly-deformed middles of thrust sheets indicate that the normal faults were not generated in the Alleghanian orogeny. Some growth faults in the Rome Formation were reactivated and show combined features of both synsedimentary and lithifield normal faulting.

During the Alleghanian orogeny, early extensional fractures, mostly veins, developed at variable angles to bedding in the hanging wall rocks. Subsequent deformation rotated or folded the veins (Figs. 3c–e) depending on their original orientations relative to the subsequent shortening direction. Similarly, no penetrative cleavages formed in the early deformation phase in the footwall rocks, as the major deformation mechanism was fracturing. During subsequent deformation, Floyd shale in footwalls of Pell City and Coosa faults formed mylonites. Veins from early fractures are incorporated as light-colored augens and ribbons aligned along mylonitic foliation. In samples from the unfoliated Floyd shale (Mf3) section in the middle of the Coosa thrust sheet where bedding is still preserved, one sees comparable sequence of more ductile sigmoidal veins overprinted in the early, regularly spaced, thin en échelon veins (Figs. 4a & b).

S_1 surfaces in the weakly-deformed limestone and siltstone from the hanging wall of the Pell City fault (F_5), where S_0 still exists, are solution cleavage. In contrast, in Floyd shales and limestones incorporated into fault zones bedding has been totally obliterated and S_1 surfaces are a mylonitic foliation. S_1 surfaces developed at variable angles to bedding, ranging from 0° to 90° (Figs. 4c–e). Even where parallel to bedding, S_1 surfaces are detectable because ooids and bedding stylolites have been flattened. Fold axial plane cleavage was observed in a fold hinge (Fig. 4e). In dolomite, cataclastic deformation was always dominant, and no S surfaces formed. The S_1 surfaces are very prominent in Floyd shale mylonite in footwalls of Pell City fault and F_7, where S_1 foliation and quartz calcite augens and ribbons (Figs. 5a & b) have totally replaced bedding and other previous structures. Quartz and calcite in augens and ribbons from early veins were recrystallized (Fig. 5b), and chlorite and illite are aligned parallel to the foliation. In limestone samples close to the Pell City and Coosa faults, S_1 surfaces are defined by elongated calcite grains with twins (Figs. 5c & d) that were fractured (Fig. 6a) or folded (Fig. 6b) by further deformation. Relicts of S_0 stylolites were folded to accommodate the grain-shape fabric (Figs. 5c & d). Unlike the shale mylonites, recrystallization of calcite (Tapp & Wickham 1987) or matrix (Schmid *et al.* 1981, Schmid 1982) was not observed in the limestone. In contrast, dolomite formed cataclasite (Figs. 6c & d) and ultracataclasite in fault zones.

In some mylonites of Floyd Formation, S_1 surfaces are modified, truncated, or folded by subsequent shear surfaces, axial surfaces of secondary isoclinal folds, and crenulation cleavage, indicating further progressive deformation. The relative sequence of microstructures is summarized in Fig. 7.

SPATIAL VARIATIONS OF DEFORMATION MECHANISMS

A qualitative survey indicates that the occurrence of microstructures and deformation mechanisms varies among different lithologies, across major thrust faults, and with distance from major thrust faults. Synsedimentary and early hard-rock normal faults are observed only in the weakly-deformed samples. In most samples from units above the Pell City faults (F_5), bedding and bedding stylolites are well preserved in siltstone, limestone, shale, and in some dolomite. Below F_5, S_0 is seen only in samples from the middle thrust sheets away from the major thrust faults. Much of the Floyd Formation in the footwalls immediately below Pell City and Coosa faults is foliated mylonite where S_0 was totally erased. The fractures and veins that formed early in the Alleghanian orogeny also have an apparent limited distribution. In weakly-deformed samples (Fig. 3c), the early fractures

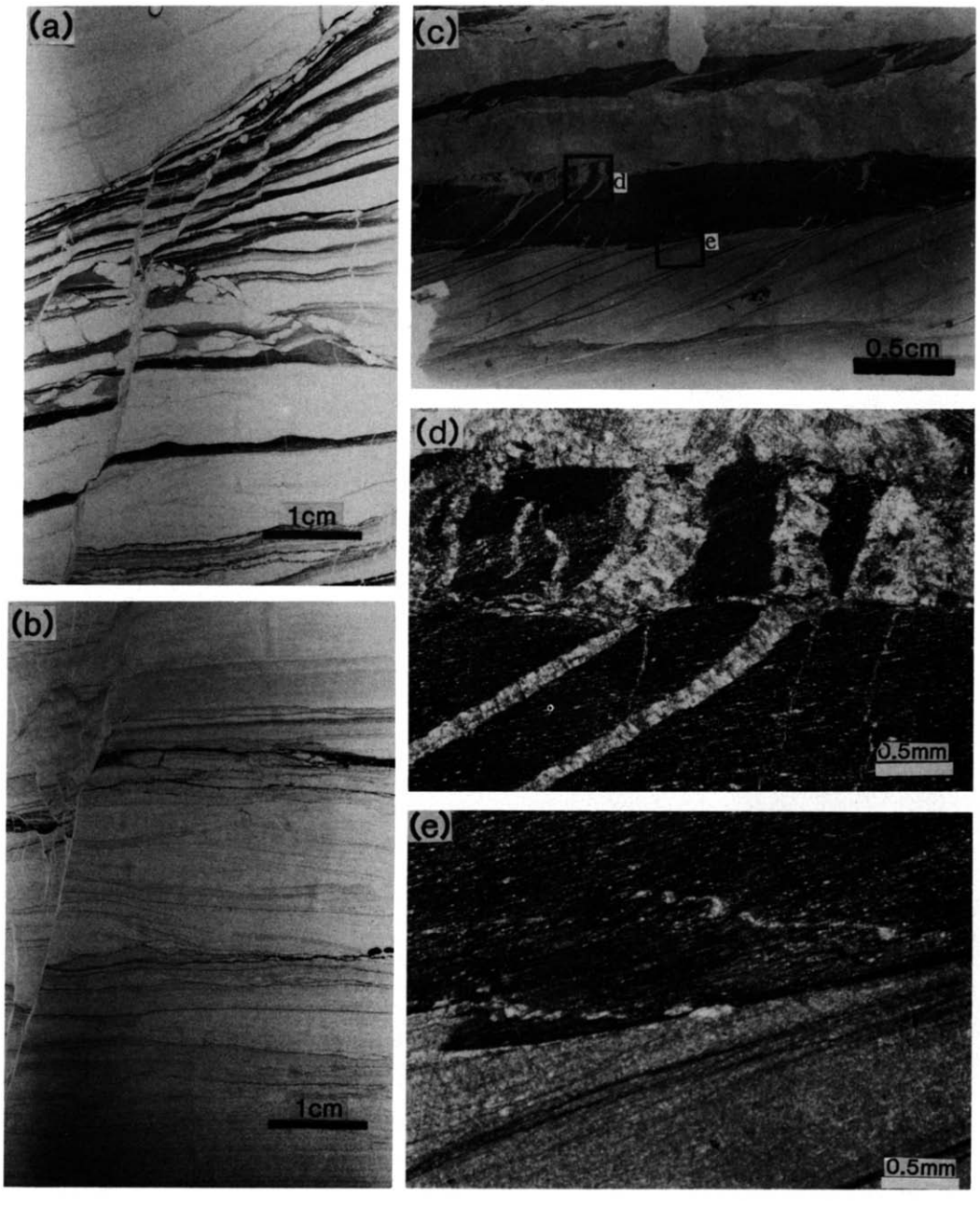

Fig. 3. (a) Synsedimentary fault (sample 937B, Rome siltstone and shale, non-polarized). (b) Normal faults in lithified rock (sample 815.7, Rome siltstone, non-polarized). (c) Earlier veins of the Alleghanian orogeny deformation were (d) sheared and (e) folded later (sample 156B, Conasauga limestone and shale, non-polarized). (d) Photomicrograph from (c) showing the sheared veins (crossed polarizers); the thin vertical veins (lower part of the photograph) are later. (e) Photomicrograph from (c) showing the folded veins (plane polarized).

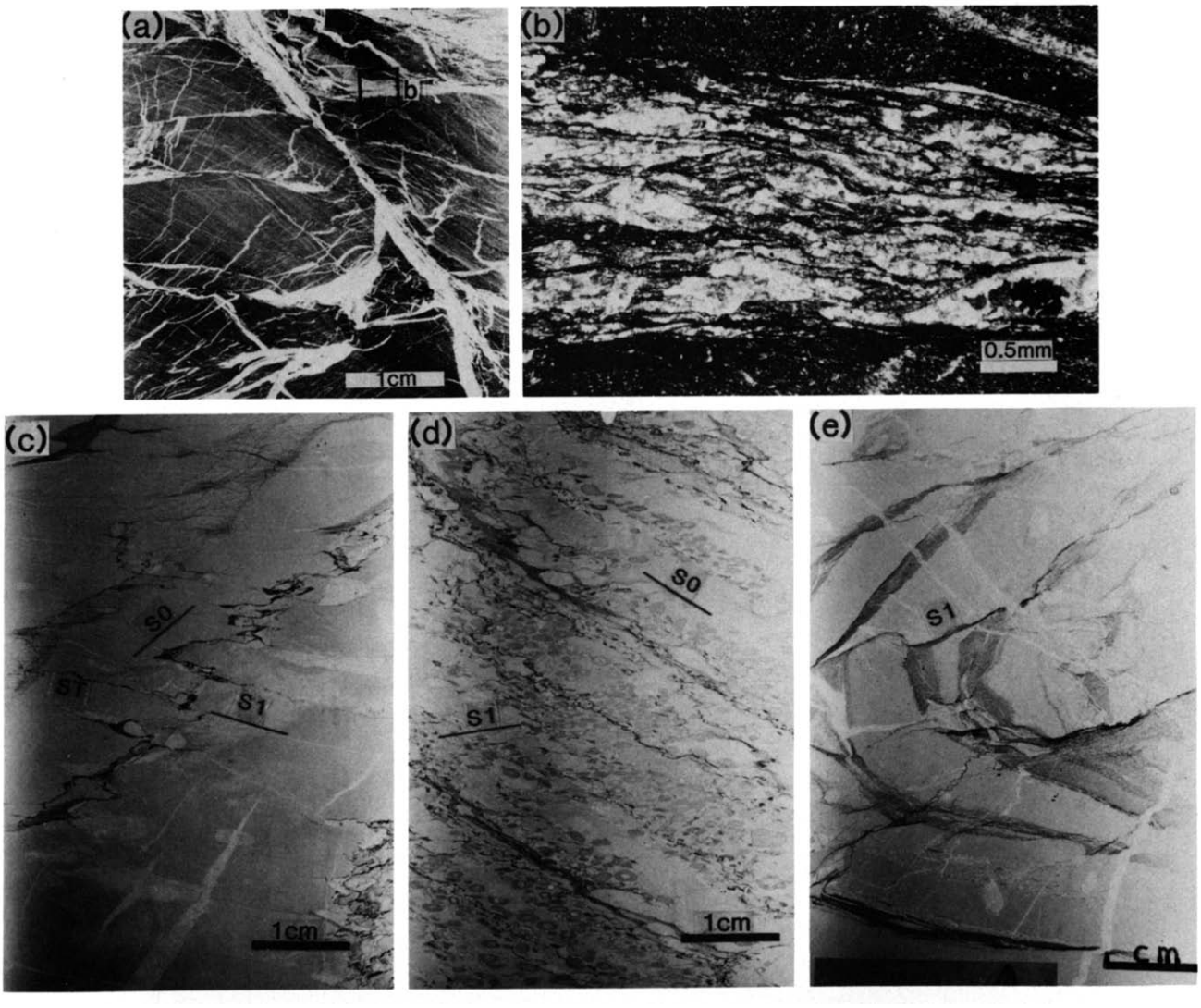

Fig. 4. (a) Thin and regularly spaced earlier en échelon veins (northeast and northwest in photograph) overprinted by thicker and irregular shear zones (sample 2039, Floyd shale, non-polarized). (b) Photomicrograph from a later shear zone (plane polarized). (c) S_0 bedding stylolites truncated by S_1 solution cleavage (sample 1021A, Conasauga limestone, non-polarized). (d) S_1 grain-shape fabric is oblique to the S_0 bedding and stylolites (sample 993, Conasauga limestone, non-polarized). (e) Fold axial plane cleavage S_1 in a fold hinge (sample 903B, Conasauga limestone, non-polarized).

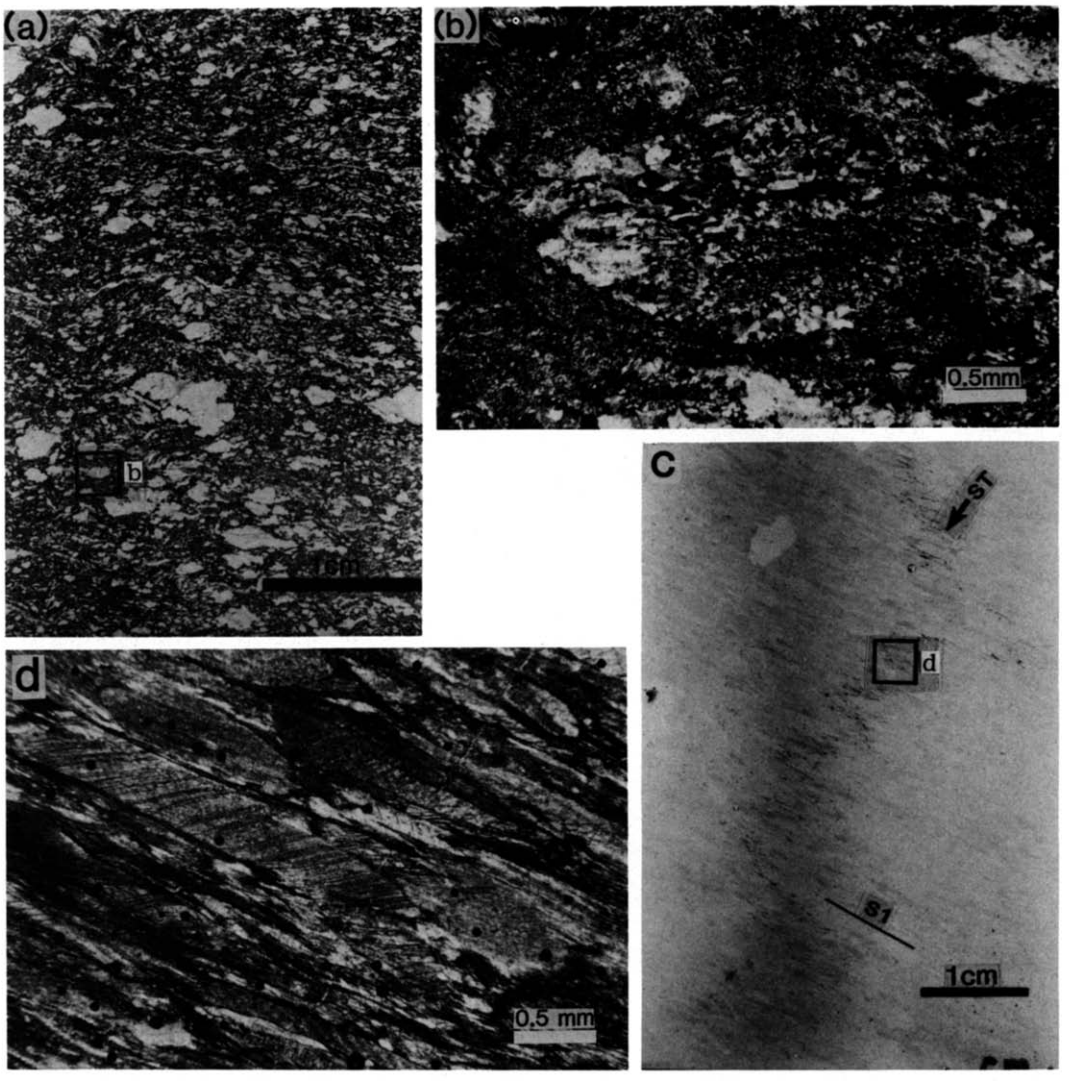

Fig. 5. (a) Shale mylonite (sample 1181F, Floyd, non-polarized); foliation formed by aligned clay minerals and light-colored augens. (b) Photomicrograph of an augen in photograph (a), showing recrystallized quartz (q) and calcite (c) (crossed polarizers). (c) S_0 bedding stylolite (ST) folded during formation of S_1 foliation (sample 2897A, Floyd limestone, non-polarized). (b) Photomicrograph from (c) showing S_1 foliation formed by elongated calcite grains (crossed-polarizers).

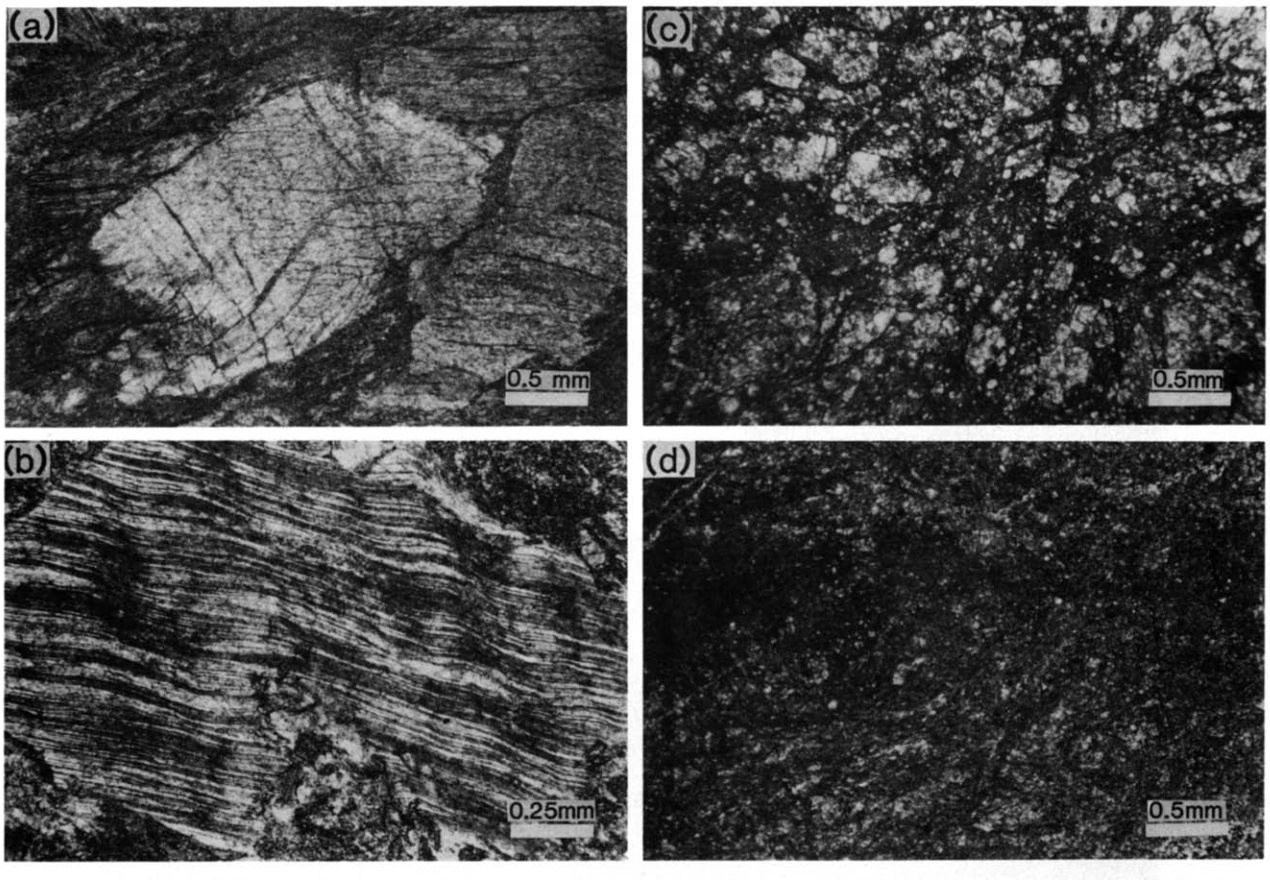

Fig. 6. (a) Photomicrograph of Floyd limestone mylonite. Calcite grains showing fractures along twin planes (sample 2122A). (b) Photomicrograph of folded twinned calcite grains (sample 2057, Floyd limestone). (c) Photomicrograph of protocataclasite, tectonic matrix <50% (sample 1173, Conasauga dolomite). (d) Photomicrograph of cataclasite, tectonic matrix >50% (sample 2588, Knox dolomite). All under crossed polarizers.

Episode	Microstructures
Preorogeny	Bedding (So) Bedding stylolites (So) Soft-sediment folds Synsedimentary faults Lithified-rock normal faults
Alleghanian orogeny	Veins (earlier, folded & faulted later) Thrust faults Bedding slip faults Solution cleavage (S_1) Axial solution cleavage (S_1) Mylonitic foliation (S_1) Cataclasites and protocataclasites Fractures Veins (later) Mylonites Recrystallization texture Folded stylolites Crenulation cleavage (S_2) Isoclinal folds (folded S_1)

Fig. 7. Observed microstructures in the core from the American Anniston No. 1 well. The overall sequence in the list is from earlier to later.

are difficult to distinguish from those formed later. In the highly-deformed samples (Figs. 5a & b), they were obliterated in the later deformation. In the later phase of Alleghanian deformation, S_1 surfaces formed as solution cleavage in limestone and siltstone above the Pell City fault and as mylonitic foliation in footwalls of major thrusts. Dolomite is deformed by cataclastic mechanisms regardless of its structural position.

To detect changes in deformation mechanisms in the Alleghanian orogeny, a point-count method was used to determine quantitatively the relative abundance of different microstructures. Point-count traverses were spaced at 2–4 times the point spacing along a single traverse with 300 points for each section. Point spacing along traverses was approximately equal to the average grain diameter. Points were tabulated within six categories. Points at which grains are undeformed, have undulatory extinction or are twinned together with sedimentary matrix constitute category I. This category contains little information about changes in deformation mechanisms, because twinning and undulatory extinction are observable only in coarse-grained rocks. These features cannot be observed in an equivalently-deformed fine-grained rock. Discontinuities such as extensional fractures, veins and faults were counted in category II. Matrix produced by cataclasis was counted in category III. Bedding-parallel stylolites of either compaction (e.g. Wong & Oldershaw 1981) or tectonic origin (Rutter 1976, Groshong *et al.* 1984, Engelder & Marshak 1985) were counted in category IV. Bedding-oblique stylolites of tectonic origin were counted in category V. Subgrains and recrystallized grains were counted in category VI (Table 2) for the extent of crystal-plastic deformation. For the typical percentage ranges of 1–8, 8–25, 25–75 and 75–92% (Table 2), the 2 SD errors for the sample size of 300 are 1–3, 3–5, 5–6 and 3–5% at a 95% confidence level (Van Der Plas & Tobi 1965).

Both limestone and dolomite samples from fault zones contain abundant cataclastic deformation (category II plus category III in Table 2) and less abundant pressure solution (category V in Table 2, Fig. 8) when compared with the thrust sheet samples. Outside of fault zones, pressure solution is much more abundant in limestone than dolomite. Shale and siltstone in fault zones have higher percentages of pressure solution than in thrust sheets (Fig. 9a), but cataclastic deformation is almost equivalent to that in thrust sheets. The second relationship is consistent with the inference that a substantial number of the fractures and veins from the thrust-sheet samples formed early, whereas they were altered or obliterated by later plastic deformation in the fault-zone samples. Plastic deformation dominates shale and siltstone from fault zone, as indicated by mylonitization and related recrystallization (Fig. 9b).

Changes in deformation mechanism among different rock types from fault zones and thrust sheets are shown in Fig. 10. For the samples from the thrust sheets, shale and siltstone have percentages of cataclastic microstructures, mainly fractures and veins, equal to or greater than those in limestone and dolomite; their percentages of pressure solution microstructures are lower than those of limestone and dolomite (Fig. 10a). Limestone samples have wider range of percentages of cataclastic deformation than dolomite, but percentages of pressure solution microstructures are consistently higher in limestone (Fig. 10a). Among the fault-zone samples, the shale and siltstone were deformed plastically, as indicated by recrystallized quartz and calcite in mylonite augens and increased grain size and alignment of clay minerals in the matrix; microstructures indicating cataclastic deformation are less abundant (Fig. 10b). In fault-related limestone, plastic deformation dominated as indicated by extensive twinning and grain-shape elongation of calcite. Fault-related dolomite was deformed by cataclasis, commonly forming cataclasite and protocataclasite. In Fig. 10(b), the abundances of cataclastic microstructures in limestone and dolomite are equivalent, primarily because the mylonitic matrix in limestone and cataclastic matrix in dolomite are counted in the same category. Different categories would distinguish between these two matrix types.

STRAIN ANALYSIS

Many limestone samples from the Conasauga Formation in the thrust sheet above the Pell City fault (F_5) are oolitic or pisolitic. The ooids and pisoids show only slight deformation in samples far from the fault, but close to the fault ooids and pisoids are substantially flattened. These ooids and pisoids provide ideal strain markers (Cloos 1947) for the R_f/ϕ strain analysis method (Dunnet 1969, Ramsay & Huber 1983, Lisle 1985). Other strain markers used here for the R_f/ϕ

method were calcite grains in myonitic limestone (see Fig. 6a), quartz and calcite augens in shale mylonite, quartz grains and dolomite grains. Many of these strain markers were previously used for the R_f/ϕ method (for example, Mancktelow 1981, Jensen 1984, Law *et al.* 1984, Odling 1984, Burg 1986, Law 1986). Mylonite augens (see Fig. 5) may only provide a lower strain limit because augens and ribbons were recrystallized, and individual augens may be disaggregated ribbons. A major advantage of the R_f/ϕ method is that it can distinguish the tectonic strain (the axial ratio R_s) from the initial ellipticity (R_i) of the grain shape (Ramsay & Hubber 1983, Lisle 1985).

Twenty samples were analyzed with 100 markers where possible and a minimum of 50 otherwise (Table 3). The vector mean ϕ, harmonic mean of R_f were calculated using the equations of Lisle (1985, p. 14). An index of symmetry is calculated for a symmetry test, and a chi-square test is used to determine the best-fit theta curves from R_s values.

The strain results are given in Table 3 and plotted in Fig. 11. The bedding displayed in Fig. 11 as short line pairs refers the side walls of the drill core as being vertical, actual strikes unknown. In samples where bedding is totally obliterated or absent, the line pair for bedding is omitted. The overall strain pattern strongly indicates the significance of the two major thrust faults. Strain magnitudes increase towards them in both hanging wall and footwall (Fig. 11). Samples from the middles of thrust sheets have tectonic strains (R_s) less than

Table 2. Abundance of microstructures

Sample	I*	II*	III*	IV*	V*	VI*	Sample location
Limestone samples:							
156	93.0	3.3	0.0	0.0	3.7	0.0	thrust sheet
903	88.0	3.0	4.3	0.0	4.7	0.0	thrust sheet
993	94.3	0.0	0.0	0.0	5.7	0.0	thrust sheet
2184	87.3	10.0	0.0	0.0	2.7	0.0	thrust sheet
1043	75.3	8.0	0.7	0.0	16.0	0.0	thrust sheet
1063	75.7	0.0	0.0	0.0	16.0	0.0	thrust sheet
575	82.3	4.3	3.3	0.0	0.0	0.0	fault zone (F_2)
972	70.7	6.7	22.3	0.0	0.3	0.0	fault zone (F_4)
1157	82.3	8.7	7.3	0.0	1.7	0.0	fault zone (F_5)
1164	75.3	9.0	13.3	0.0	2.3	0.0	fault zone (F_5)
2743	64.0	7.7	28.3	0.0	0.0	0.0	fault zone (F_7)
2897	68.7	4.0	25.3	0.3	1.7	0.0	fault zone (F_7)
Dolomite samples:							
727	94.0	1.0	0.0	3.7	1.3	0.0	thrust sheet
1604	94.3	1.0	1.7	0.0	3.0	0.0	thrust sheet
1634	94.3	1.7	0.0	1.3	2.7	0.0	thrust sheet
1636	96.0	0.0	0.0	2.0	2.0	0.0	thrust sheet
1775	92.3	2.3	0.0	4.3	1.0	0.0	thrust sheet
1793	92.0	4.0	0.0	2.0	2.0	0.0	thrust sheet
2468	94.7	2.3	0.0	1.0	2.0	0.0	thrust sheet
1665	48.0	5.3	43.3	2.0	1.3	0.0	local fault
450	92.3	4.7	3.0	0.0	0.0	0.0	fault zone (F_1)
575	92.7	3.7	1.0	2.0	0.7	0.0	fault zone (F_2)
585	85.7	5.0	7.3	2.0	0.0	0.0	fault zone (F_2)
862	94.3	3.7	1.7	0.0	0.3	0.0	fault zone (F_3)
885	93.7	3.0	1.3	1.3	0.7	0.0	fault zone (F_3)
969	65.0	9.0	21.7	0.0	1.7	2.7	fault zone (F_4)
972	55.7	11.3	25.3	0.7	1.3	5.7	fault zone (F_4)
1173	63.7	10.3	25.3	0.0	0.3	0.3	fault zone (F_5)
1179	82.7	7.7	6.3	2.3	1.0	0.0	fault zone (F_5)
2588	73.0	12.3	10.0	3.0	1.7	0.0	fault zone (F_7)
Shale and siltstone:							
401	85.0	5.0	0.0	9.7	0.3	0.0	thrust sheet
505	91.0	0.0	0.0	8.7	0.3	0.0	thrust sheet
637	98.0	0.7	0.0	0.7	0.7	0.0	thrust sheet
655	82.0	11.7	0.0	2.3	1.3	0.0	thrust sheet
778	95.7	0.7	0.0	3.7	0.0	0.0	thrust sheet
1502	95.7	1.3	0.0	0.0	1.3	2.7	thrust sheet
1523	84.7	6.3	1.3	1.3	1.0	5.3	thrust sheet
1893	90.3	3.0	0.7	5.7	0.3	0.0	thrust sheet
2039	79.0	17.3	0.0	1.3	0.0	2.3	thrust sheet
2268	91.3	5.0	0.7	2.0	1.0	0.0	thrust sheet
432	54.0	9.0	0.0	0.7	2.0	4.3	fault zone (F_1)
1181	56.0	3.7	0.0	0.0	4.3	36.0	fault zone (F_5)
1199	77.7	4.7	0.0	0.0	2.0	15.7	fault zone (F_5)
1253	70.7	1.3	0.0	0.0	4.0	24.0	fault zone (F_5)
2644	58.7	8.7	1.7	0.0	2.0	29.0	fault zone (F_7)
2687	69.3	7.3	0.0	0.0	3.7	19.7	fault zone (F_7)

*I: Undeformed and slightly deformed; II: Fractures; III: Cataclasite; IV: Bedding-parallel stylolite; V: Bedding-oblique stylolite; VI: Recrystallization.

the initial ellipticity (R_i) of the strain markers. In contrast, strains near faults reach 5.5 and commonly exceed 2.0. The fluctuation (F), which is the range of ϕ (refer to Ramsay & Huber 1983), is 180° in thrust sheets (Table 3), whereas close to the faults, the fluctuation is very small, in a range of 35–65°. Lithologically, shale-derived mylonites yield the largest strain magnitudes, mylonitic limestones yield the next largest magnitudes, and dolomites yield the lowest strain magnitudes although cataclastic phenomena are common there.

Although the R_f/ϕ results are consistent with the occurrence of the large faults, the strain magnitudes may still be underestimated, especially in samples with significant tectonic matrix. The R_f/ϕ method only measures shape modification of markers and does not record spatial changes among markers as might be accommodated by tectonic matrix.

DISCUSSION

Most strain ellipses are either at low angles or parallel to bedding (Fig. 11). This strain pattern could indicate either simple shear on bedding, pure shear, or a combination of the two (Sanderson 1982, Kusky & De Paor 1991), or non-coaxial non-laminar flow (Lister & Snoke 1984). Simple shear may be important during thrust fault initiation, because bedding-slip faults are observed in the upper part of the hanging wall of the Pell City fault (sample 993), and the early veins were rotated (Fig. 3c). When large strains were generated by displacement along major thrust faults, simple shear may not be the only deformation process. The folded veins (Fig. 3e), bedding-parallel and low-angle solution cleavage and conjugate shear zones (Fig. 4a) indicate that pure shear was important in the later deformation phase with a shortening direction at a high angle to bedding. If observed low-angle and bedding-parallel strain ellipses were mainly caused by simple shear followed by pure shear, then most units in the core are substantially stretched, such as the bedding flattening strain observed by Holst (1985). However, if simple shear parallel to the thrust transport direction is the only mechanism, then original formation thicknesses would not change even for large strains (W. M. Dunne 1992 personal communication). More data are needed to distinguish the deformation mechanisms in mylonites.

Early Alleghanian deformation was dominated by cataclastic mechanisms, producing fractures, microfaults and veins with some solution stylolites. This deformation affected all rock types. However, more veins occur in shale and limestone than dolomite. Abundant crystal-plastic microstructures and penetrative surfaces

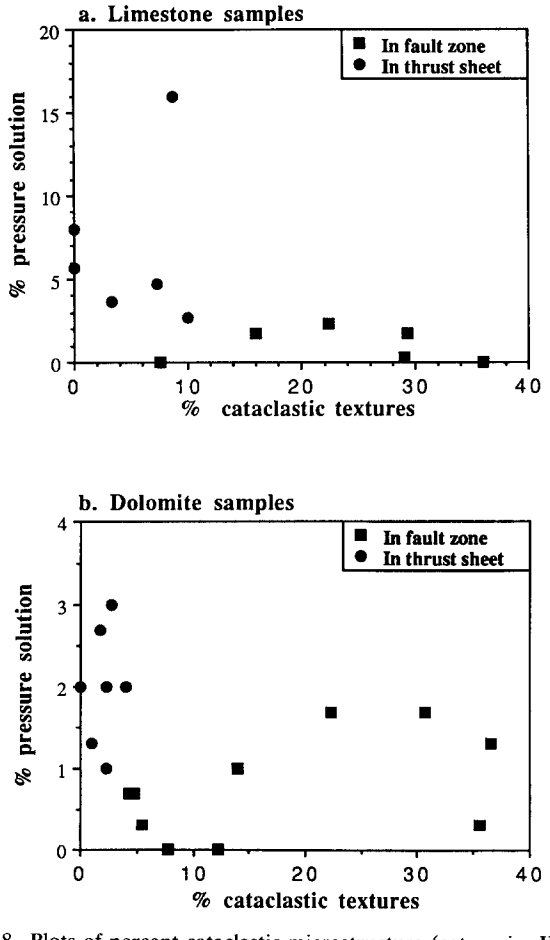

Fig. 8. Plots of percent cataclastic microstructure (categories II and III in Table 2) vs percent pressure-solution microstructures (category V in Table 2). (a) Limestone samples. (b) Dolomite samples.

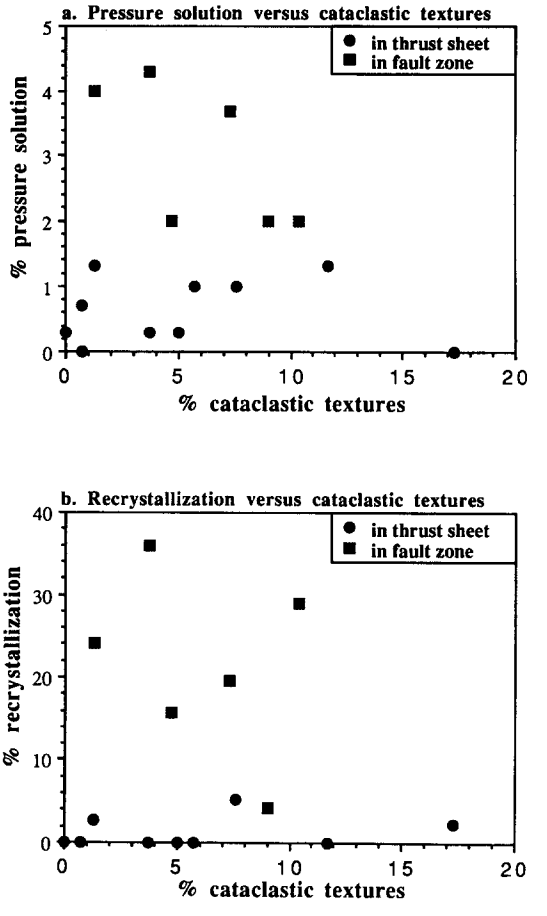

Fig. 9. Plots for shale and siltstone samples. (a) Percent cataclastic microstructures (II and III in Table 2) vs percent pressure-solution microsturctures (V in Table 2). (b) Percent cataclastic microstructures vs percent recrystallization microstructures.

(S_1) formed during subsequent deformation, overprinting or even obliterating early structures. Deformation mechanisms changed across major faults and by rock types. Dolomite was deformed by cataclastic mechanisms in both fault zones and in thrust sheets. Fault-related dolomite has formed cataclasite and protocataclasite. Fault-related limestone was dominated by plastic deformation and formed mylonite. Pressure solution was more prominent in limestone units within thrust sheets than in the fault-related limestone. Shale and siltstone outside of fault zones were deformed by extensional fracturing and pressure solution. The fault-related shale and siltstone are characterized by mylonitization.

In shales, siltstone and limestone, cataclastic processes gave way to plastic processes during thrust sheet emplacement for both fault zones and thrust sheets. The cataclastic–plastic transition is not everywhere obvious in thrust sheets, because of the later overprinting structures. For example, the quartz–calcite augens and ribbons in the mylonitic Floyd Formation are not sedimentary clasts because original grain size is very fine. Instead, cataclastic deformation produced calcite and quartz-filled fractures (Figs. 12a–d), and the later plastic deformation deformed the veins forming augens and ribbons (Figs. 12e & f). This interpreted cataclastic–plastic transition could have been caused by change in deformation conditions such as strain rate, confining pressure, temperature and water content (Rutter 1974, Groshong 1988, Knipe 1989). The small thrust faults F_1–F_4 did not produce tectonites like those in the footwalls of the major faults. Tectonic burial and the grain-size reduction caused by the large displacement along the major thrust faults are believed to be the principal factors that cause a transition from brittle to plastic deformation or frictional sliding to ductile flow (White *et al.* 1980, Mitra 1984, Gilotti & Kumpulainen 1986).

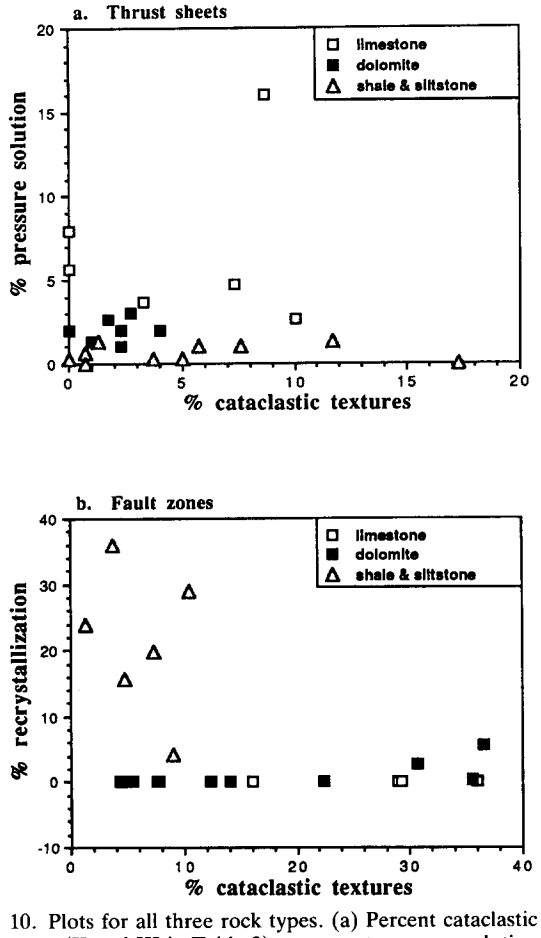

Fig. 10. Plots for all three rock types. (a) Percent cataclastic microstructures (II and III in Table 2) vs percent pressure-solution microstructures for thrust-sheet samples. (b) Percent cataclastic microstructures vs percent recrystallization microstructures for fault samples.

A deformation-mechanism association is defined by Groshong (1988) as the deformation mechanisms formed for the same environmental conditions in the same rock type. Tectonites are in Groshong's association IV, which is subdivided into glide tectonites (IVG), dominated by glide mechanisms, and recrystallization tectonites (IVR), dominated by recrystallization. A tectonite front of type IVR occurs in shale and siltstone at about 360 m (1180 ft) below the present land surface. A tectonite front of type IVG in limestone occurs at about 670 m (2200 ft) below the current land surface. An equivalent tectonite front in dolomite was not reached in the core. These observations are comparable with Mitra's (1987) tectonic fronts in the central Appalachians. The tectonite fronts in limestone and shale are about at the same structural position, which is located along the leading edge of the North Mountain thrust sheet (Mitra 1987, pp. 588–589). The equivalent limestone and shale tectonite front in the southern Appalachians in Alabama appears at the surface to the southeast of the well position, near the Talladega thrust (Fig. 1) (Carrington 1973, Guthrie 1987, 1990). In three dimensions, the observations from the core combined with the surface geology indicate a northwesterly-tilted tectonite-front surface. The same pattern has also been observed in central Appalachians (Evans & Dunne 1991).

The major thrust faults in the core have a similar configuration in terms of rock types, that is, a limestone–dolomite package in the hanging wall and a shale–siltstone package in the footwall. A schematic thrust model is constructed for this rock-type configuration (Fig. 13) in association with microstructure development. Initially (Fig. 13a), fractures formed during thrust fault initiation. During emplacement of the thrust sheets (Figs. 13b & c), different rock types behaved differently because of the differences in physical compositions, burial depths, and structural positions (also see Fig. 10). The ductile structures in shale and limestone overprinted brittle structures, whereas dolomite developed only cataclasite.

The strain pattern and strain partitioning among cataclastic deformation, pressure solution, and plastic deformation across the major thrusts faults are synthesized in Fig. 14. Data in Fig. 14 are based on measurements from Pell City and Coosa faults (Fig. 11, Tables 2 and 3). Both the hanging wall and footwall have increasing strain magnitude towards the fault. Maximum measured strain magnitudes in the footwall are twice the

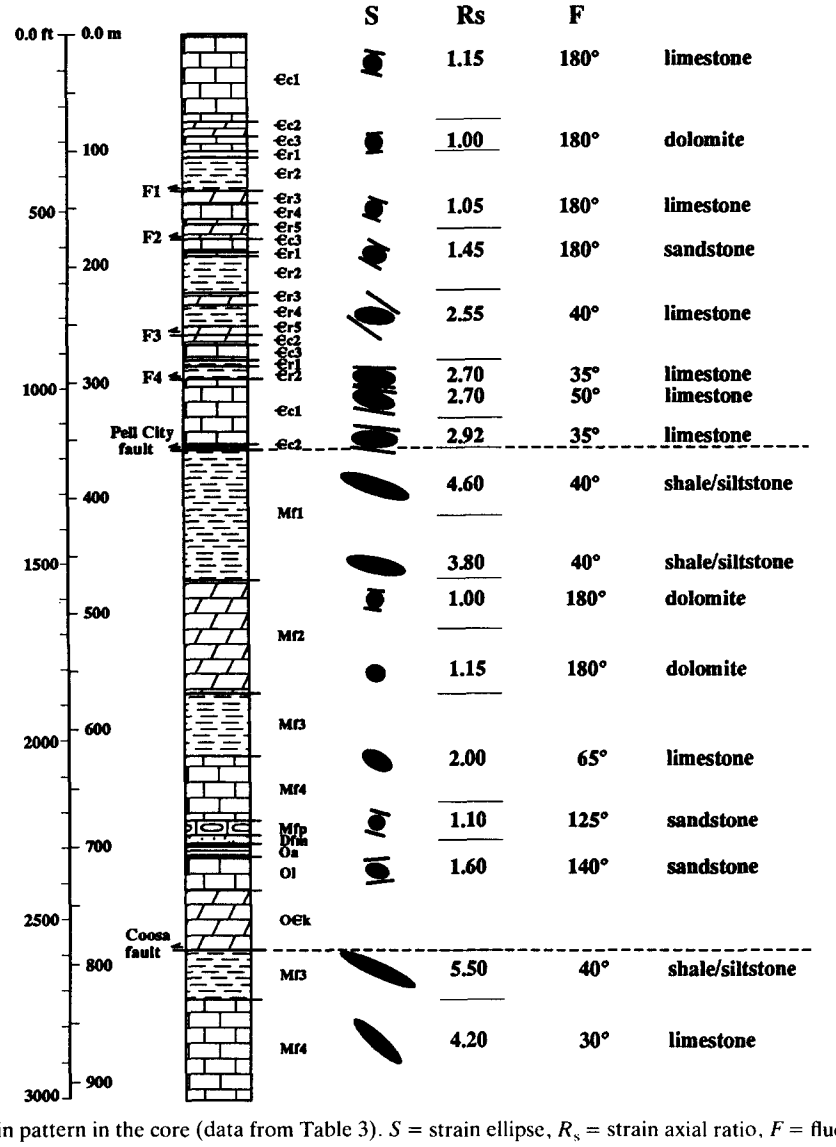

Fig. 11. Strain pattern in the core (data from Table 3). S = strain ellipse, R_s = strain axial ratio, F = fluctuation.

Table 3. Strain data (R_f/ϕ method)

Sample	R_s*	R_i†	χ^2‡	F§	S_0‖	N¶	Measurements and rock type
67	1.25	1.50	16.76	180	30	102	Calcite ooids, limestone
73.5	1.15	1.50	8.50	180	12	101	Calcite ooids, limestone
302.2	1.00	1.17	18.40	180	7	102	Dolomite ooids, dolomite
592	1.05	1.45	17.77	180	−22	106	Dolomite ooids, limestone
617	1.45	1.50	18.40	180	−26	103	Quartz grains, sandstone
993	2.55	1.50	9.83	40	−34	100	Ooids and pellets, mudstone
978	2.70	1.50	8.40	35	−2	104	Ooids and pellets, mudstone
1031	2.70	1.75	22.80	50	−7	100	Calcite ooids, limestone
1063	2.30	1.50	4.63	45	−30	102	Calcite ooids, limestone
1110	2.85	1.80	13.20	150	−24	52	Pellets, limestone
1114.5	2.92	1.75	12.00	35	−8	101	Ooids and pellets, limestone
1279	4.60	1.62	22.00	40	none	52	Augens and ribbons, mylonite
1554	3.80	1.75	20.00	40	none	100	Augens and ribbons, mylonite
1604	1.00	1.69	6.80	180	15	50	Dolomite grains, dolomite
1089	1.15	1.50	10.07	180	none	106	Quartz grains, dolomite
2057	2.00	1.62	5.27	65	none	104	Calcite grains, limestone
2230	1.45	1.50	11.80	125	−19	100	Quartz grains, sandstone
2363	1.60	1.65	18.80	140	8	102	Quartz grains, sandstone
2644	5.50	1.75	13.20	40	none	50	Augens and ribbons, mylonite
2845	4.20	1.75	3.88	30	none	102	Calcite grains, limestone

*R_s: strain ellipse ratio.
†R_i: initial ellipse ratio.
‡χ^2: critical value of chi-squared test.
§F: fluctuation.
‖S_0: bedding.
¶N: sample size.

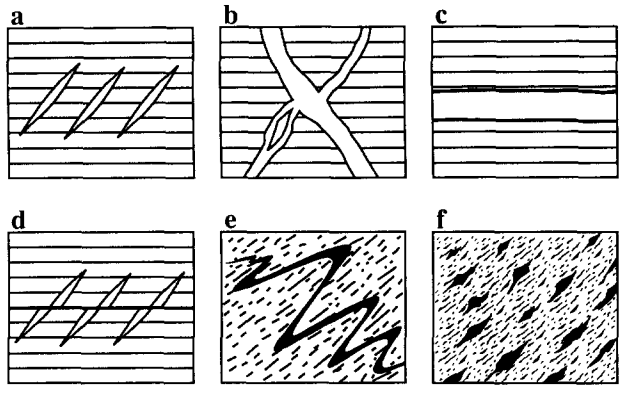

Fig. 12. Sequential deformation of Floyd shale. Various veins are formed during the earlier cataclastic deformation: (a) en échelon, (b) conjugate and (c) bedding parallel. Bedding is represented by solid lines. In the later deformation, the earlier veins are (d) faulted or (e) folded, which can be seen within thrust sheets. Solution cleavage (dashed lines in e) accompanied folding. In fault zones, veins are deformed in a ductile manner and formed augens and ribbons (f), in which quartz and calcite are recrystallized. The thin irregular short lines represent foliation, which is defined by aligned clay minerals and solution seams.

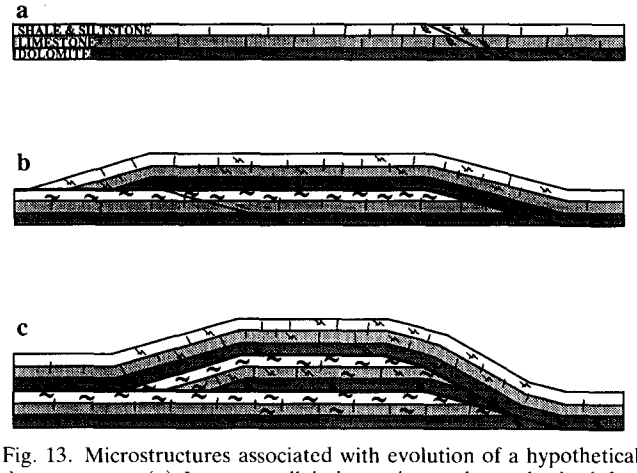

Fig. 13. Microstructures associated with evolution of a hypothetical thrust system. (a) Layer parallel shortening and cataclastic deformation during initiation of thrust faults. (b) & (c) The earlier fractures are overprinted by solution cleavage, cataclasite, mylonitic foliation, etc., during emplacement of thrust sheets.

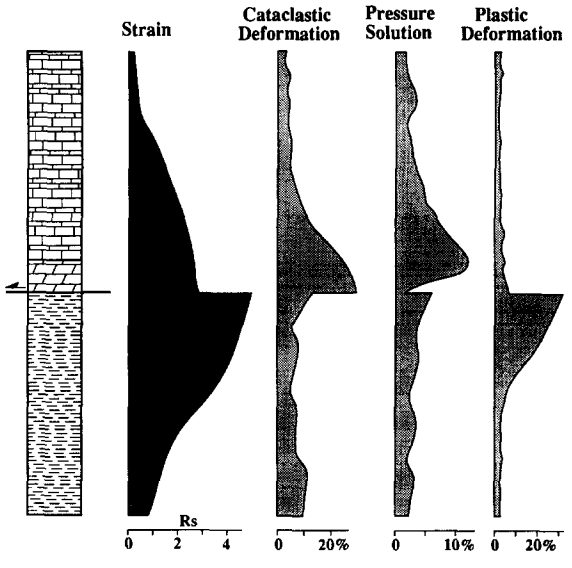

Fig. 14. Strain and strain partioning data synthesized across the two major faults. Strain magnitude is based on the axial ratio (R_s, strain in dolomite is extrapolated from trend), cataclastic deformation includes fracturing and faulting, plastic deformation includes recrystallization and twinning. Three rock types in the schematic stratigraphic column are limestone, dolomite and shale–siltstone (rock-type symbols are the same as in Fig. 2).

strain magnitudes measured in the hanging wall. The partitioning of strain in the hanging wall is quite different from the footwall. Cataclastic deformation and pressure solution caused greatest strain in the hanging wall, and are less important in the footwall. A cataclastically deformed hanging wall is also a typical feature of thrust sheets exposed in the southern Appalachian fold–thrust belt (Wojtal 1986, Wojtal & Mitra 1986, 1988). In contrast, plastic deformation accommodated most strain in the footwall and is less important in the hanging wall (Fig. 14).

CONCLUSIONS

Microstructural analysis of the rocks from the American Anniston No. 1 core revealed two deformation episodes. Soft-sediment folds, growth faults and normal faults in lithifield rocks formed in a pre-orogenic episode. In the Alleghanian orogeny, early fractures were overprinted by subsequent deformation that produced S_1 solution cleavage and mylonitic foliation.

Deformation mechanisms change among different rock types. Dolomite is characterized by cataclastic deformation in both fault zones and thrust sheets. Fault-related dolomite formed cataclasite and protocataclasite. Fault-related limestone is dominated by plastic deformation and formed mylonite. Pressure solution is more prominent in limestone in thrust sheets than in fault-related limestone. Shale and siltstone outside of fault zones were deformed by fracturing and pressure solution. Fault-related shale and siltstone are characterized by mylonitization. Foliated tectonites in shale and siltstone dominated by recrystallization occur at 360 m (1180 ft) below the current surface. Foliated tectonites in limestone dominated by translation gliding occur at about 670 m (2200 ft) below the current surface. Dolomite tectonites are not present in the core.

Finite strain magnitudes increase towards major faults in both hanging walls and footwalls. The axial ratio (R_s) of strain ellipse reaches 2.92 in fault-related limestone, and 5.5 in mylonitic shale. Among the major rock types in the core, dolomite has the minimum ductile strain, with R_s values ranging from 1.0 to 1.15. Limestone has moderate ductile strain, with R_s values ranging from 1.15 to 2.92. Sandstone has a limited R_s range (around 1.10–1.60). Shale and siltstone developed the largest ductile strain, with R_s values ranging from 3.8 to 5.5. For measuring thickness of deformed units and for drawing balanced cross-sections, finite strain should be taken into consideration, especially in the inner part of the fold–thrust belt.

In a thrust model with limestone–dolomite in the hanging wall and the shale–siltstone in the footwall, strain in the hanging wall is mostly caused by cataclastic

deformation and pressure solution. Strain in the footwall is mostly caused by plastic deformation.

Acknowledgements—This work represents a portion of the dissertation research at the University of Alabama. Amoco Production Company provided the core and funding for this study. I thank Ron Nelson for facilitating for both. Betsy J. Dransfield, Dan J. Patterson and Richard H. Groshong selected and cut the thin-section blocks. The manuscript has been greatly improved by many reviews and comments from Richard H. Groshong, and careful reviews by William A. Thomas, Harold H. Stowell, Albert W. Shultz, John H. Spang, William Dunne, Gautam Mitra and Roger C. Brewer. It also has been benefited from the reviews and suggestions of Steven F. Wojtal and an anonymous reviewer.

REFERENCES

Burg, J.-P. 1986. Quartz shape fabric variations and *c*-axis fabrics in a ribbon-mylonite: arguments for an oscillating foliation. *J. Struct. Geol.* **8**, 123–131.

Carrington, T. J. 1973. Metamorphosed Paleozoic sedimentary rocks in Chilton, Shelby and Talladega Counties, Alabama. In: *Talladega Metamorphic Front*, A Guidebook to the 11*th Annual Fieldtrip of the Alabama Geological Society* (edited by Carrington, T. J.). Alabama Geological Society.

Chester, F. M. 1989. Dynamic recrystallization in semi-brittle faults. *J. Struct. Geol.* **11**, 847–858.

Cloos, E. 1947. Oolite deformation in the South Mountain fold, Maryland. *Bull. geol. Soc. Am.* **58**, 843–918.

Dunnet, D. 1969. A technique of finite strain analysis using elliptical particles. *Tectonophysics* **7**, 117–136.

Engelder, J. T. & Marshak, S. 1985. Disjunctive cleavage formed at shallow depths in sedimentary rocks. *J. Struct. Geol.* **7**, 327–343.

Evans, M. A. & Dunne, W. M. 1991. Strain factorization and partitioning in a foreland thrust sheet. *J. Struct. Geol.* **13**, 21–35.

Fellows, R. E. 1943. Recrystallization and flowage in Appalachian quartz. *Bull. geol. Soc. Am.* **54**, 1399–1432.

Gibson, R. G. & Gray, D. R. 1985. Ductile-to-brittle transition in shear during thrust sheet emplacement, Southern Appalachian thrust belt. *J. Struct. Geol.* **7**, 513–525.

Gilotti, J. A. & Kumpulainen, R. 1986. Strain softening induced ductile flow in the Sarv thrust sheet, Scandinavian Caledonides. *J. Struct. Geol.* **8**, 441–455.

Groshong, R. H., Jr. 1988. Low temperature deformation mechanisms and their interpretation. *Bull. geol. Soc. Am.* **100**, 1329–1360.

Groshong, R. H., Jr., Pfiffner, O. A. & Pringle, L. R. 1984. Strain partitioning in the Helvetic thrust belt of eastern Switzerland from the leading edge to the internal zone. *J. Struct. Geol.* **6**, 5–18.

Guthrie, G. M. 1987. *Geologic Map of Parts of Talladega*, Shelby Chilton and Coosa Counties. Filemap, Geological Survey of Alabama.

Guthrie, G. M. 1990. Contrasts in structural styles and deformation mechanisms in the foreland–hinterland transition zone, central Alabama Appalachians. In: *Contrasts in Structural Styles and Mechanisms in a Foreland–Hinterland Transition Zone, Central Alabama Appalachians, A Guidebook for Fieldtrip II* (edited by Guthrie, G. M. & Osborne, W. E.). Alabama Geological Survey, Tuscaloosa, Alabama, 17–34.

Hanmer, S. 1989. Initiation of cataclastic flow in a mylonite zone. *J. Struct. Geol.* **11**, 751–762.

Harper, G. D. 1985. Tectonics of slow spreading mid-ocean ridges and consequences of variable depth to the brittle–ductile transition. *Tectonics* **4**, 379–394.

Holst, T. B. 1985. Implications of a large flattening strain from the origin of a bedding parallel foliation in the Early Proterozoic Thomson Formation, Minnesota. *J. Struct. Geol.* **7**, 375–383.

Jensen, L. N. 1984. Quartz microfabric of the Laxfordian Canisp Shear zone, N.W. Scotland. *J. Struct. Geol.* **6**, 293–303.

Knipe, R. J. 1989. Deformation mechanisms—recognition from natural tectonites. *J. Struct. Geol.* **11**, 127–146.

Kusky, T. M. & De Paor, D. G. 1991. Deformed sedimentary fabrics in metamorphic rocks: evidence from the Point Lake area, Slave province, Northwest Territories. *Bull. geol. Soc. Am.* **103**, 486–503.

Law, R. D. 1986. Relationships between strain and quartz crystallographic fabrics in the Roche Maurice quartzites of Plougastel, Western Brittany. *J. Struct. Geol.* **8**, 493–515.

Law, R. D., Knipe, R. J. & Dayan, H. 1984. Strain path partitioning with thrust sheets: microstructural and petrofabric evidence from the Moine Thrust Zone at Loch Eriboll, northwest Scotland. *J. Struct. Geol.* **6**, 477–497.

Lisle, R. J. 1985. *Geological Strain Analysis, A Manual for the* R_f/ϕ *Method*. Pergamon Press, Oxford.

Lister, G. S. and Snoke, A. W. 1984. S–C mylonites. *J. Struct. Geol.* **6**, 617–638.

Lopez, J. A. 1984. Southern Appalachian thrust/fracture study (Joy Mfg., American Anniston #1 corehole; Calhoun Co., Alabama). AMOCO Production Company joint project, Tulsa research department/New Orleans regional office, Res. Rep. No. F84-G-26.

Mancktelow, N. S. 1981. Strain variation between quartz grains of different crystallographic orientation in a naturally deformed metasiltstone. *Tectonophysics* **78**, 73–84.

Marshak, S. & Engelder, T. 1985. Development of cleavage in limestones of a fold–thrust belt in eastern New York. *J. Struct. Geol.* **7**, 345–359.

Miller, E. L., Gans, P. G. & Garing, J. 1983. The Snake Range décollement; an exhumed mid-Tertiary brittle–ductile transition. *Tectonics* **2**, 239–264.

Mitra, G. 1984. Brittle to ductile transition due to large strains along the White Rock thrust, Wind River Mountains, Wyoming. *J. Struct. Geol.* **6**, 51–61.

Mitra, G. & Yonkee, W. A. 1985. Relationship of spaced cleavage to folds and thrusts in the Idaho–Wyoming thrust belt. *J. Struct. Geol.* **7**, 361–373.

Mitra, S. 1987. Regional variations in deformation mechanisms and structural styles in the central Appalachian orogenic belt. *Bull. geol. Soc. Am.* **98**, 569–590.

Odling, N. E. 1984. Strain analysis of strain path modeling in the Loch Tollie gneisses, Gairloch, N.W. Scotland. *J. Struct. Geol.* **6**, 543–563.

Powell, C. McA. & Rickard, M. J. 1985. Significance of the early foliation at Bermagui, N.S.W. Australia. *J. Struct. Geol.* **7**, 385–400.

Ramsay, J. G. & Huber, M. I. 1983. *The Techniques of Modern Structural Geology, Volume* 1: *Strain analysis*. Academic Press. London.

Rutter, E. H. 1974. The influence of temperature, strain rate and interstitial water in the experimental deformation of calcite rocks. *Tectonophysics* **22**, 311–334.

Rutter, E. H. 1976. Kinetics of rock deformation by pressure solution. *Phil. Trans. R. Soc. Lond.* **A283**, 203–219.

Rutter, E. H. 1986. On the nomenclature of mode of failure transitions in rocks. *Tectonophysics* **122**, 381–387.

Sanderson, D. J. 1982. Models of strain variation in nappes and thrust sheets: a review. *Tectonophysics* **88**, 201–233.

Schmid, S. M. 1982. Microfabric studies as indicators of deformation mechanisms and flow laws operative in mountain building. In: *Mountain Building Processes* (edited by Hsu, K. J.). Academic Press, London, 95–110.

Schmid, S. M., Casey, M. & Starkey, J. 1981. The microfabric of calcite tectonites from the Helvetic napes (Swiss Alps). In: *Thrust and Nappe Tectonics* (edited by McClay, K. R. & Price, N. J.). *Spec. Publs geol. Soc. Lond.* **9**, 151–158.

Sibson, R. H. 1977. Fault rocks and fault mechanisms: *J. geol. Soc. Lond.* **133**, 191–213.

Stearns, D. W. 1969. Fracture as a mechanism of flow in naturally deformed layered rocks. In: *Conference on Research in Tectonites* (edited by Bear, A. J. & Norris, D. K.). *Geol. Surv. Pap. Can.* **68-52**, 79–90.

Szabo, M. W., Osborne, W. E., Copeland, C. W., Jr. & Neathery, T. L. 1988. *Geologic Map of Alabama*, 1:250,000. Geological Survey of Alabama, Tuscaloosa.

Tapp, B. & Wickham, J. 1987. Relationships of rock fabrics to incremental and accumulated strain in the Conococheague Formation, U.S.A. *J. Struct. Geol.* **9**, 457–472.

Thomas, W. A. 1972. Mississippian stratigraphy of Alabama. *Ala. geol. Surv. Monogr.* **12**.

Thomas, W. A. 1985. Chapter IV—Northern Alabama Section. In: *Valley and Ridge Thrust Belt: Balanced Structural Sections*, Pennsylvanian to Alabama (edited by Woodward, N. B.). *Dep. geol. Sci., Univ. of Tennessee Stud. Geol.* **12**, 54–61.

Thomas, W. A. 1989. The Appalachian fold–thrust belt in Alabama. In: *Contrasts in Style of American Thrust Belts*, 28*th International Geological Congress Field Trip Guidebook T*380 (edited by Thomas, W. A., Viele, G. W., Platt, L. B. & Schmidt, C. J.).

Tullis, J. A. & Yund, R. A. 1987. Transition from cataclastic flow to

dislocation creep of feldspar. Mechanisms and microstructures. *Geology* **15**, 606–609.
Turner, F. J. & Weiss, L. E. 1963. *Structural Analysis of Metamorphic Tectonites*. McGraw-Hill, New York.
Van Der Plas, L. & Tobi, A. C. 1965. A chart for judging the reliability of point counting results. *Am. J. Sci.* **263**, 87–90.
Watts, M. J. & Williams, G. D. 1979. Fault rocks as indicators of progressive shear deformation in the Guingamp region, Brittany. *J. Struct. Geol.* **1**, 323–332.
White, W. H., Burrows, S. E., Carreras, J., Shaw, N. D. & Humphreys, F. J. 1980. On mylonites in ductile zones. *J. Struct. Geol.* **2**, 175–187.
Williams. P. F. 1985. Multiply deformed terrains—problems of correlation. *J. Struct. Geol.* **7**, 269–280.
Wilson, C. J. L. & de Hedouville, P. 1985. Early cleavage development in the Late Ordovician of northeast Victoria, Australia. *J. Struct. Geol.* **7**, 401–408.
Wise, D. U., Dunn, D. E., Engelder, J. T., Geiser, P. A., Hatcher, R. D., Kish, S. A., Odom, A. L. & Schamel, S. 1984. Fault-related rocks: suggestions for terminology. *Geology* **12**, 391–394.
Wojtal, S. 1986. Deformation within foreland thrust sheets by populations of minor faults. *J. Struct. Geol.* **8**, 341–360.
Wojtal, S. & Mitra, G. 1986. Strain hardening and strain softening in fault zones from foreland thrusts. *Bull. geol. Soc. Am.* **97**, 674–687.
Wojtal, S. & Mitra, G. 1988. Nature of deformation in some fault rocks from Appalachian thrusts. In: *Geometries and Mechanisms of Thrusting with Special Reference to the Appalchians* (edited by Mitra, G. & Wojtal, S.). *Spec. Pap. geol. Soc. Am.* **222**, 17–33.
Wong, P. D. & Oldershaw, A. 1981. Burial cementation in the devonian, Kaybob Reef Complex, Alberta, Canada. *J. sedim. Petrol.* **51**, 507–520.
Wu, S. & Groshong, R. H., Jr. 1991. Low-temperature deformation of sandstone, southern Appalachian fold–thrust belt. *Bull geol. Soc. Am.* **103**, 861–875.